Scientific Paper

The Effect of Annealing on Structural, Optical and Electrical Properties of Nanostructured Tin Doped Indium Oxide Thin Films

Mohammad Hossein Habibi* and Nasrin Talebian

Department of Chemistry, University of Isfahan, Isfahan, 81746-73441, Iran

Received 05-09-2004

Abstract

A low level tin doped indium oxide, ITO, (ca. 10 w % SnO_2) thin films were prepared on glass substrate by electron beam technique. Deposited films with deposition rate of 0.1–0.25 nm s^{-1} were annealed at different temperatures from 250 to 550 °C in air. The thin films were characterized using low and high angle X-ray diffraction and UV-visible spectroscopy. The lattice constant and the grain size of ITO thin film were 10.118 Å and 36 nm, respectively. UV-visible transmission spectra confirmed the formation of high quality ITO nano-particles. These low level tin doped indium oxide thin films showed higher transparency over the visible wavelength region (ca. 95%) than those of already reported with higher level tin doped indium oxide thin films deposited at 350 °C. The transmission data were used for direct and indirect optical band gap calculations ca. 3.6 and 3.8eV, respectively. The refractive index and porosity of ITO films annealed at different temperature were calculated from measured transmittance data. The results showed that the refractive index of thin films increased with increasing annealing temperature, but the porosity of ITO thin films showed opposite trend. The lowest resistivity (2.9×10^{-6} Ω m) and highest porosity (40.1%) were obtained for the annealed film at 550 °C.

Keywords: Nanostructure ITO, low and high angle XRD, UV-visible transmission spectra, annealing, electron beam evaporation.

Introduction

Metal oxide thin films like indium oxide and tin doped indium oxide have unique characteristics such as good conductivity, high optical transmittance over the visible wavelength region, excellent adhesion to substrates and chemical stability and photochemical properties. These properties are resulted from their n-type semiconductor behavior and wide band gaps. Therefore, indium oxide and tin doped indium oxide are used in a wide range of applications including solar energy conversion and photovoltaic devices, flat panel displays and biocatalytic redox transformation.[1–3] New applications require ITO films with lower resistivity and higher optical transmissions over the visible wavelength region. In order to obtain optimal characteristic i.e. high transparency and low sheet resistance, the parameters such as thickness of the film, dopant type and its amount and the other deposition conditions have to be optimized. Haacke defined a figure of merit quantity to specify the quality of transparent conductor.[4] It is well known that the electrical and optical properties of semiconducting oxides like In_2O_3 depend strongly on defect density created by external doping or disturbed stoichiometry as well as their preparation and growth conditions.[5] Tin (Sn) is one of the suitable external dopants among the various doping elements such as F, Cl, Sb.[6] When trying to get low resistivity ITO films, the amount of doping of tin (Sn) should be properly controlled. It is worth to note that the substitution of tin element within In_2O_3 lattice is also important. If tin substitute with indium, it liberates a free electron into the lattice and the electrical conduction will increase but it also acts as a neutral impurity scattering center and decreases the electrical conduction when combined with interstitial oxygen atoms.[7] In_2O_3 thin films have been deposited by a number of techniques such as dc magnetron sputtering,[8] RF sputtering,[9] CVD,[10] sol-gel,[11] thermal evaporation,[12] and spray pyrolysis.[13] In spite of good potential of ITO thin films prepared by electron beam evaporation technique, less attention has been paid to the study of annealing temperature effect on its structural, electrical and optical properties. Furthermore, the investigations on a number of nanocrystalline

ITO thin films have demonstrated peculiar features of optical behavior of nanostructured films as compared with those of compact polycrystalline or single-crystal ones. These features are related both to the quantum-sized effect and the strong influence of the surface atoms, the number of which is comparable to those located in crystalline core.

In the previous reports the dependence of the above mentioned properties were investigated on the substrate temperature,[14] vapor pressure and the presence of ion beam irradiation,[15] thickness of films,[16]deposition rate,[17] tin doping level[18] and deposition parameters at all[19–20] and it has been less attention paid to the effect of annealing temperature for thin films deposited by electron beam evaporation. The aim of present work is to pay more attention to study of the annealing temperature influences on the structural characteristics, optical and electrical behaviors of low level tin doped indium oxide nanostructured thin films prepared by electron beam evaporation technique.

Experimental

Sample preparation

An electron beam evaporation system similar to those shown in Figure1 was used for film deposition. The evaporation conditions were: (1) a vacuum of 4.2 $\times$ 10^{-5} mbar; (2) an accelerating voltage of 1–10 kV; (3) electron beam current 10–12 mA and the rate of evaporation were controlled within the range 0.1–0.25 nm/s. The thickness of thin film was controlled by using a quartz crystal thickness monitor, resulting in films having 45 nm. The target material used in this study was an ITO pellet (purchased from Merck) with a composition of In_2O_3 89.75 wt%, SnO_2: 9.82 and trace amount of other oxides which are determined by XRF analysis CaO: 0.12, K_2O: 0.096, Fe_2O_3: 0.069, CuO: 0.069, Al_2O_3: 0.025, ZnO: 0.025 and UO_2: 0.026. Glasses slides were immersed both in boiling sulfuric acid and Milli-Q water for 30 min and afterward they ultrasonically cleaned in acetone and absolute EtOH for 5 min. Finally they were rinsed with water. The substrate temperature during the deposition process was kept at 25 °C. The phase composition of ITO films annealed at different temperatures were characterized using XRD technique with a D8 Advanced Bruker X-ray diffractometer at room temperature, with monochromated CuK_α (λ =1.54 Å) in the scan range of 2θ between 4° to 100° with a step size of 0.03 (2θ/s). Measurements were taken under beam-acceleration conditions of 40 kV/35 mA. The UV-visible optical transmission spectra of the thin films were recorded by a double-beam spectrophotometer Cary 500 scan. The sheet resistance of films was measured by four-probe method at room temperature.

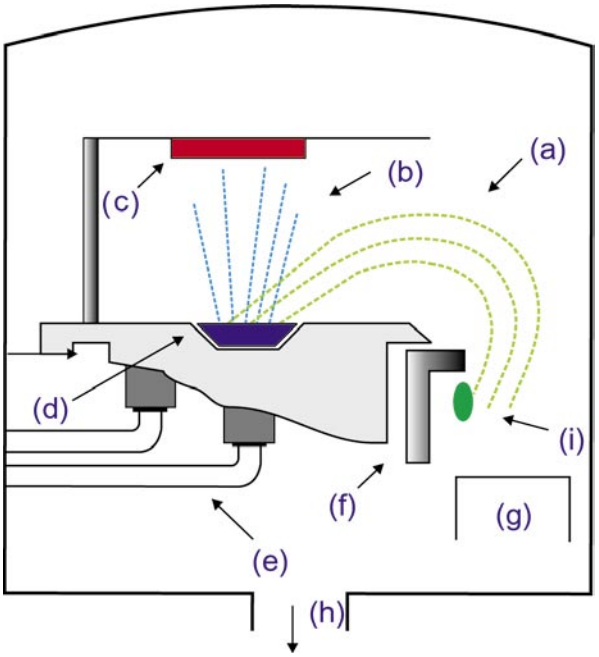

Figure 1. Electron beam evaporation set up used for thin films preparation; (a) Electron Beam, (b) Material Vapor, (c) Substrate, (d) Target Material, (e) Water Cooling Lines, (f) Shield, (g) Magnet, (h) To Vacuum Pump, (i) Tangstan Filamen.

Results and discussion

XRD measurements

Typical low-angle XRD spectra of the tin doped In_2O_3 thin films before and after heat treatment at ca. 550 °C were shown in Figures 2 and 3, respectively. As it can be seen from Figure 2, before heat treatment ill-defined amorphous phase is appeared but after heat treatment, the well-defined structure of the multi layers is evident from the large number of peaks in the XRD pattern (Figure 3). Figure 4 shows the high angle XRD pattern for as-deposited thin film. It can be found that before heat treatment only one less significant shoulder appears in the 2θ between 20° and 30°. The low intensity of this feature suggests that this film consists of amorphous phase up to 450 °C. Figure 5 shows the variation of XRD patterns with annealing temperatures. The annealed film pattern at ca. 550 °C matches with In_2O_3 reference peaks as body-centered cubic form which was observed as bar graphs in Figure 6. The figures clearly showed a change with annealing from a single broad amorphous peak centered 2θ = 30° to a set of sharp, well-defined peaks positions expected the primitive cubic lattice crystal structure with a 10.118 Å lattice parameter. In particular, the line at 2θ=30.581° corresponds to the reflection from the (222) plane is close to the position of strongest line of the reference indium oxide. The other peaks were due to reflections from the (400), (431) and (440) planes. None of the

Table1. Comparison between measurement XRD results and standard pattern for In_2O_3 samples annealed at 550 °C for 24 h.

Observed 2θ (degree)	Standard 2θ (degree)	h	k	l
27.858	–	3	1	0
30.581	30.578	2	2	2
41.842	41.860	3	3	2
52.709	52.73	4	3	3
63.668	63.71	4	4	4

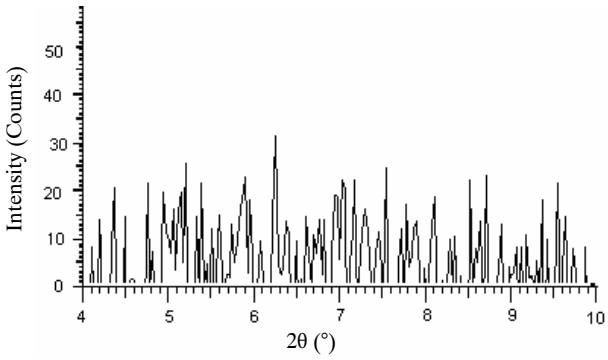

Figure 2. Low angle-XRD pattern of tin doped In_2O_3 sample before annealing.

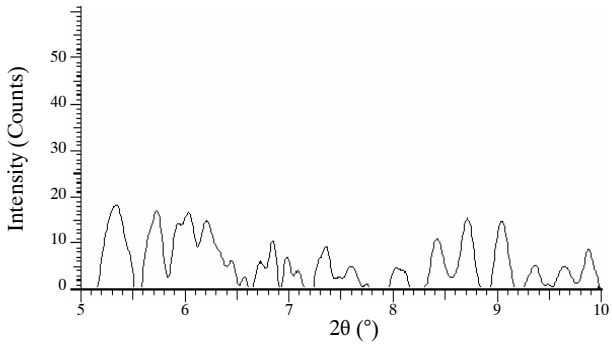

Figure 3. Low angle XRD pattern of tin doped In_2O_3 sample after annealing (550 °C).

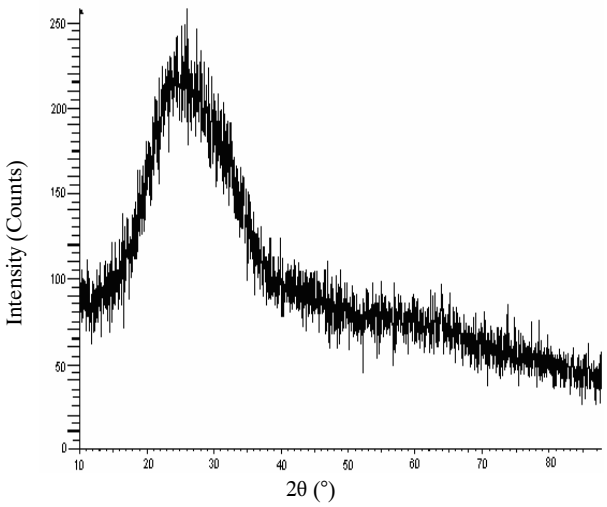

Figure 4. High angle-XRD pattern of tin doped In_2O_3 sample before annealing.

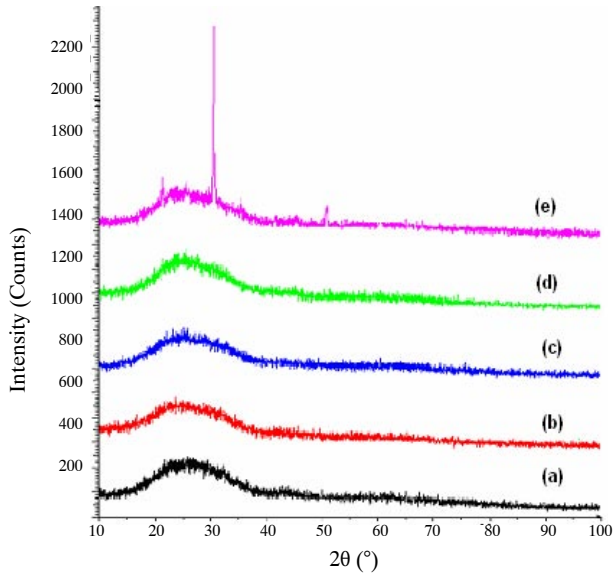

Figure 5. High angle-XRD pattern of tin doped In_2O_3 sample at different annealing temperatures: (a) as-deposited, b) 250, c) 350, d) 450, and e) 550 °C.

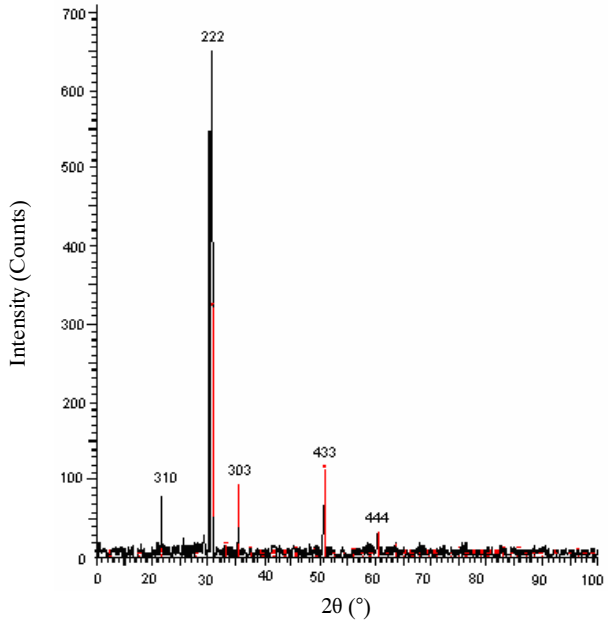

Figure 6. High angle-XRD pattern of tin doped In_2O_3 sample after annealing at 550 °C. The bar graphs represents XRD pattern of In_2O_3 sample.

spectra indicated any characteristic peaks of Sn, SnO and/or SnO_2, which means that the tin atoms were doped substitutionally into the In_2O_3 lattice.[6] In continuum, we also used the FWHM of line about 0.320 degree to calculate crystal size according to Debye-Scherrer formula[21] which it was ca. 36 nm. A comparison between measurement XRD results and standard pattern for In_2O_3 were shown in Table 1.

Electrical property

A sharp drop in resistivity was observed in the annealing temperature range between 250 and 450 °C. The obtained lowest resistivity was 2.9×10^{-6} Ω.m at 450 °C, which could be attributed to improved crystalline nature of film during annealing. The more increase in temperature shows no further effect on resistivity (not shown here). The electrical property of the films was found to be related to the microstructure and crystallographic structure, which in turn strongly depend on the annealing temperature.

Optical transmittance

The transparency of thin films for all temperatures exhibits a sharp decrease in about the UV region as shown in Figure 7. Transmission percent of ITO films was also changed from ca. 10 to 95% for as-deposited and annealed at 550 °C, respectively. The ripples in the spectrum resulted from the interference light, since they show wave forms that are characteristic of the Interference light.[22] Further, there was a shift in adsorption edges to shorter wavelength with annealing temperature up to 550 °C which was due to the Burstien–Moss shift[23] and/or it could also be related to the quantum-size effect.[24]

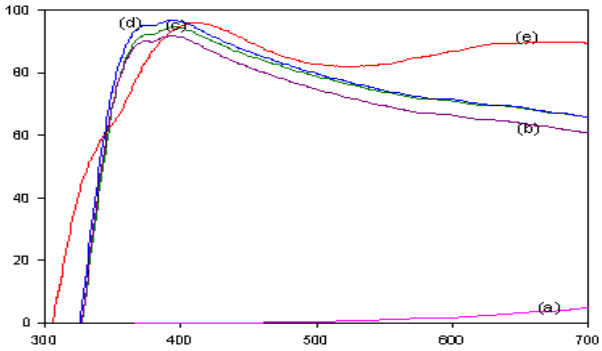

Figure 7. Optical transmission *vs.* wavelength of light for low tin doped In_2O_3 thin film: (a) as-deposited, (b) annealed at 250, (c) 350 (d) 450, and (e) 550 °C.

Refractive index and porosity

The refractive index of prepared ITO films was calculated from the measured transmittance spectrum. The evaluation method used is based on the analysis of the transmittance spectrum of a weakly absorbing film deposited on a non-absorbing substrate.[25] The refractive index n(λ) over the spectral range is calculated by using the envelopes that are fitted to the measured extreme. See Equations 1 and 2, where n_o and n_s are the refractive index of air and films respectively, T_{max} is the maximum envelope, and T_{min} is the minimum envelope. The porosity of the ITO thin films was calculated using the equation 3,[26] where n_d is pore-free ITO which is taken to be 1.8. It should be noted that the refractive index of ITO ranging from 1.8 to 2.1 in the UV-NIR region.[27–31] The calculated refractive index and porosity of ITO films are listed in table 2. The results showed that the refractive index was increased from 1.57 to 1.61 by increasing annealing temperature up to 450 °C and then was decreased by further increasing of annealing temperature which is due to crystallinity improvement. On the other hand, the porosity showed opposite trend and its maximum value (40.1%) was observed for ITO thin film annealed at 550 °C.

$$n(\lambda) = \sqrt{S + \sqrt{S^2 - {n_0}^2(\lambda){n_S}^2(\lambda)}} \quad (1)$$

$$S = \frac{1}{2}(n^2{}_o(\lambda)+n^2{}_s(\lambda))+2n_0 n_s\left(\frac{T_{max}(\lambda)-T_{max}(\lambda)}{T_{max}(\lambda)\times T_{max}(\lambda)}\right) \quad (2)$$

$$\text{Porosity} = [1 - \frac{n^2-1}{n^2{}_d-1}] \times 100(\%) \quad (3)$$

$$\alpha = \frac{\ln(1/T)}{d} \quad (4)$$

Table 2. Refractive index and porosity of ITO films annealed at different temperatures.

Annealing temperature (°C)	Refractive index	Porosity (%)
250	1.57	34.6
350	1.59	31.3
450	1.61	28.9
550	1.53	40.1

Estimation of ITO band-gap

A given material can exhibit a direct or indirect band to band transitions depend on its crystal structure. For example, Si single crystals have an indirect transition located at 1.1 eV. In contrast, the amorphous Si is characterized by a direct optical transition with a larger Eg value. In addition, both types of transitions can also be seen in the same material simultaneously, for example GaP. In order to distinguish between direct and indirect transitions usually uses adsorption depths which given by 1/α. Ignoring the reflectivity, which is expected to be low, the absorption coefficient (α) can be determined from the film transmission, T, as shown in equation 4, where d is the thickness of the film in nm. The adsorption depth for direct transition span the 100–1000 nm range while in the indirect transition case this quantity can be as large as 10^4 nm.[32] With regarding this criterion, the adsorption depth versus incident photon energy plot was shown in Figure 8. It can be seen that the indirect transitions were most probable than the direct transitions. In order to obtain more insight

into origin of transitions, we used the other graphical method as follows. The direct and indirect allowed-forbidden band-gaps of the ITO films may roughly be estimated by plotting the $(\alpha h\nu)^n$ versus $h\nu$ ($n=2$ for allowed direct, $n=1/2$ for allowed indirect, $n=1/3$ for forbidden indirect and $n=2/3$ for forbidden direct optical transitions) and extrapolating the linear region of the plot toward low energies.[33] Figure 10 represents these plots for the In_2O_3 electrodes heated at 550 °C. Extrapolating the linear parts of the $(\alpha h\nu)^2$ versus $h\nu$ plots (Figure 9, n=2) gives a direct band gap (E_{gd}) of 3.6 eV for the ITO film. Thus, the direct band gap estimated in the present work for the nanostructured ITO film is in a good agreement with the published values.[34–35]

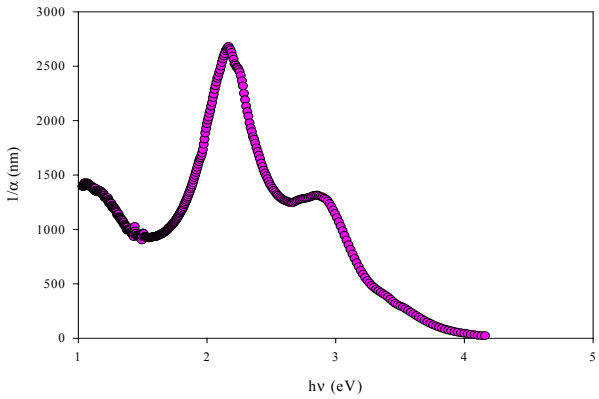

Figure 8. The adsorption depth variation *vs* incident photon energy.

A comparison of the allowed and forbidden transitions for ITO thin films which also was shown in Figure 9, indicates that the better linearization and the wider linear region are observed for the former transitions. This means that the indirect allowed transitions are realized in this film. The E_{gi} value estimated in the present work was 3.87 eV at annealing temperature 550 °C. It should be noted that for ITO thin films, it is difficult to choose what type of indirect transitions is realized really. As it can be seen in Figure 9, in order to select the most probable band to band transition, the whole transitions have been overlaid. The allowed indirect transition is the most probable transition. The Burstien-Moss shift towards higher energies is clearly seen in band gap energy values of annealed ITO thin films shown in Table 3, which has also been reported by other authors.[36]

In order to compare the Haacke figure of merit quantity ($\varphi_{TC} = T^{10}/R_s$) of many techniques, the tansmittance and resistance results of ITO thin films prepared by various methods are presented in Table 4. The results showed that a relatively good figure of merit can be obtained by electron beam evaporation technique in comparison with the others.

Electronic properties of tin doped In_2O_3 (ITO) electrode in contact with 0.1 mol dm^{-3} H_2SO_4 solution under visible light was investigated by means of linear sweep voltammetery and electrochemical impedance spectroscopy techniques.[39]

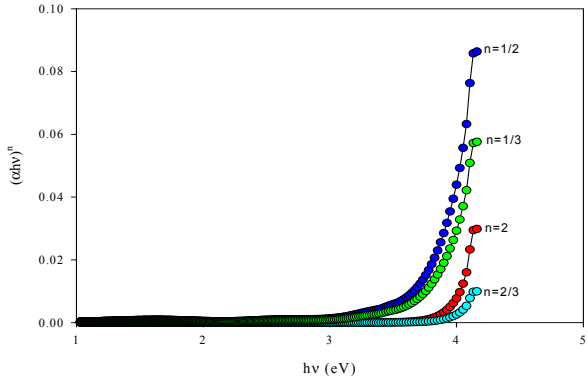

Figure 9. Comparison between allowed and forbidden direct and indirect transitions $(eV.cm^{-1} \times 10^4)^n$ in low level tin doped In_2O_3 thin film heated at 550 °C for 24 h.

Table 3. The variation of indirect band gap with annealing temperature.

Annealing temperature (°C)	E_{gi} (eV)
250	3.71
350	3.78
450	3.80
550	3.87

Surface morphology

AFM image analysis was used to reveal the particle size and surface morphology of ITO thin films annealed at different temperatures. It was found that the films consisted of nanosize crystallite with a dimension of about 10–40 nm which is increased up to 550 °C. AFM image analysis also shows the depth of about 12–20 nm for annealed ITO films at different temperatures. The films contain obvious pore structures between particles, which are decreased during annealing at higher temperatures.

Conclusions

From the obtained results following conclusions can be drawn.

1) The XRD results showed that the crystallinity of ITO thin films was improved with annealing and nanocrystalline films with 36 nm in diameter grain size obtained at 550 °C.

2) High quality film with resistivity as low as 2.9×10^{-6} Ω.m and a transmittance ca. 95% were obtained by electron beam evaporation technique.

Table 4. Comparison of ITO films characteristics prepared by different techniques.

Technique	ρ(Ω.m)	R_S (Ω. □$^{-1}$)	Transmittance in the visible region (T%)	Figure of merit (Ω / □)	Ref.
Electron beam evaporation	2.9×10^{-6}	64	95	9.3553×10^{-3}	Present work
Electron beam evaporation	3.0×10^{-6}	–	92	–	[14]
Pulsed laser deposition	4.0×10^{-6}	–	85	–	[37]
Magnetron sputtering	–	40	90	8.7170×10^{-3}	[38]

3) The calculation of ITO thin films refractive index showed that the porosity was also improved by annealing.

4) The allowed-indirect transitions were the most probable transition and the allowed-indirect optical band gap was found to vary from 3.71 to 3.87 eV with increasing annealing temperature.

5) The Haacke figure of merit quantity comparison of many techniques showed that electron beam evaporation is a promising technique for preparing of nanostructure ITO thin films.

6) Electron beam deposited tin doped In_2O_3 films annealed in air have a good potential for high conductive and transparent window applications.

7) The surface of annealed film at different temperatures reveals that the films are homogeneous, but porous, which is suitable for photocatalytic applications. The porosity improves the catalytic efficiency of the films due to increasing their effective surface area. The crystallite size was increased in the range of 10–40 nm during annealing.

Acknowledgements

We are grateful to Isfahan University Graduate School for financial support of this work.

References

1. M. Wirtz J. Kluczik, M. Rivera, *J. Am. Chem. Soc.* **2000**, *122*, 1047–1056.
2. C. A. Martinez, J. D. Stewart, *Curr. Org. Chem.* **2000**, *4*, 263–268.
3. C. G. Granquist, *Appl. A: Solids Surf.* **1993**, *57*, 19–22.
4. G. Haacke, *J. Appl. Phys.* **1976**, *47*, 4086–4089.
5. C. Liu, T. Matsutani, N. Yamamato, M. Kiuchi, *Europhys. Lett.* **2002**, *59*, 606–610.
6. J. L. Vossen, *RCA Rev.* **1671**, *32*, 289–291.
7. G. Frank, H. Kostlin, *Appl. Phys. A. Solids Surf.* **1982**, *27*, 197–200.
8. I. A. Ryzhikov, A. A. Pukhov, A. S. Il'in, *Microelectronic Eng.* **2003**, *69*, 270–273.
9. E. Bertran, C. Corbella, M. Vives, *Solid State Ionic* **2003**, *165*, 139–148.
10. M. Penza, S. Cozzi, M. Tagliente, L. Mirenghi, C. Martucci, A. Quirini, *Thin Solid Films* **1999**, *349*, 71–77.
11. S. K. Poznyak, A. I. Kulak, *Electrochimica Acta* **2000**, *45*, 1595–1605.
12. F. Zhu, C. Huan, K. Zhang, A. Wee, *J. Appl. Phys.* **1999**, *86*, 974–980.
13. K. S. Ramaiah, V. S. Raja, A. K. Bhatanagar, *Semicond. Sci. Technol.* **2000**, *15*, 676–683.
14. J. George, C. S. Menon, *Surf. Coat. Technol.* **2000**, *132*, 45–48.
15. M. Yamagushi, A. Ide-ektessabi, H. Namura, N. Yasui, *Thin Solid films* **2004**, *447–448*, 115–118.
16. M. Bender, M. Seeling, C. Danbe, H. Frankenberger, B. Ocker, J. Stollenwerk, *Thin Solid films* **1998**, *326*, 67–71.
17. A. Salehi, *Thin Solid films* **1998**, *324*, 214–218.
18. K. Manivannan, A. Subrahmanyam, *J. Appl. Phys.* **1993**, *26*, 1516–1521.
19. I. Hamberg, C. G. Granquist, *J. Appl. Phys., Lett.* **1982**, *40*, 362–367.
20. C. Liu, T. Matsutani, N. Yamamoto, M. Kiuchi, *Europhys. Lett.* **2002**, *59*, 606–610.
21. B. D. Cullity, Elements of X-Ray Diffraction, 2nd ed., Addison-Wesley, MA, 1978, p. 102–105.
22. H. Lin, S. Kumon, T. Yoko, H. Kozuka, *Thin Solid films* **1998**, *315*, 266–272.
23. E. Burstien, *Phys. Rev.* **1954**, *93*, 652–659.
24. A. V. Vorontsov, E. N. Savinov, J. Zhengsheng, *J. Photochem. Photobiol. A: Chem.* **1999**, *125*, 113–117.
25. J. C. Manifacier, J. Gasiot, J. P. Fillard, *J. Phys. E9* **1976**, 1002–1004.
26. B. E. Yoldas, P. W. Partlow, *Thin Solid Films* **1985**, *129*, 1–14.
27. M. Just, N. Maintzer, I. Blech, *Thin Solid Films* **1978**, *48*, L19–L20.
28. W. W. Molzen, *J. Vac. Sci. Technol.* **1975**, *12*, 99–105.
29. J. C. C. Fan, F. J. Bechuer, *J. Electrochem. Soc.* **1975**, *112*, 1718–1723.
30. Y. Ohhata, F. Shinoki, S. Yoshida, *Thin Solid Films* **1979**, *59*, 255–261.
31. K. Pommier, C. Gril, J. Marucchi, *Thin Solid Films* **1981**, *77*, 91–98.
32. Encyclopedia of Electrochemistry, Edited by A. J. Bard and M. Stratmann, volume 6, "Semiconductor Electrodes and Photochemistry" Willey VCH Verlag GmbH, 2002, p 25.

33. J. K. Pankove, "Optical Processes in Semiconductors", Dover Publications, 1971, Inc. Chapter 3, p 34.
34. M. J. Alam, D. C. Cameron, *Thin Solid Films* **2000**, *377–378*, 455–459.
35. Seon-Soon Kim, Se-Young Choi, Chan-Gyung Park, Hyeon-Woo Jin, *Thin Solid Films* **1999**, *347*, 155–160.
36. L. Meng, M. P. dos Santos, *Thin solid Films* **1998**, *322*, 56–62.
37. H. Kim, C. G. Gilmore, A. Pique, J. S. Horwitz, *J. Appl. Phys.* **1999**, *86*, 6451–6461.
38. J. F. Smith, A. J. Aronson, D. Chen, W. H. Class, *Thin Solid Films* **1980**, *72*, 469–474.
39. A. Hassanzadeh, M. H. Habibi, A. Zeini-Isfahani, *Acta Chim. Slov.* 2004, *51*, 507–527.

Povzetek

Komercialno uprašeno aktivno oglje je bilo uporabljeno za sorpcijo reaktivnega barvila Brillant Red HE-3B iz vodnih raztopin. Preučevan je bil vpliv pH raztopine, začetne koncentracije barvila, temperature in časa sorpcije na izčrpanje barvila. Ravnotežne sorpcijske izoterme so bile analizirane z linearnim, Freundlichovim in Langmuirjevim modelom. Najvišji korelacijski koeficienti so bili dobljeni pri Langmuirjevih izotermah. Izračunani so bili navidezni termodinamični parametri. Iz njihovih vrednosti se lahko zaključi, da je sorpcija molekul reaktivnega barvila entropijsko voden endotermen proces. Kinetika sorpcije je bila analizirana z uporabo kinetičnih modelov psevdo-prvega in psevdo-drugega reda. Iz podatkov je razvidno, da je enačba drugega reda bolj primerna, kar nakazuje, da je difuzija v delce tista stopnja, ki določa hitrost sorpcije.